Available online at www.sciencedirect.com
SCIENCE DIRECT®
ELSEVIER
Nuclear Physics A 750 (2005) 245–255
NUCLEAR PHYSICS A

Observation of the hot GDR in neutron-deficient thorium evaporation residues

J.P. Seitz [a,b,1], B.B. Back [c], M.P. Carpenter [c], I. Diószegi [d,2], K. Eisenman [b], P. Heckman [a,b,3], D.J. Hofman [e], M.P. Kelly [c], T.L. Khoo [c], S. Mitsuoka [c,4], V. Nanal [f], T. Pennington [c,✠], R.H. Siemssen [c,5], M. Thoennessen [a,b,*], R.L. Varner [g]

[a] *Department of Physics and Astronomy, Michigan State University, East Lansing, MI 48824, USA*
[b] *National Superconducting Cyclotron Laboratory, Michigan State University, East Lansing, MI 48824, USA*
[c] *Argonne National Laboratory, Argonne, IL 60439, USA*
[d] *Department of Physics and Astronomy, State University of New York at Stony Brook, Stony Brook, NY 11794, USA*
[e] *Department of Physics, University of Illinois at Chicago, Chicago, IL 60607, USA*
[f] *Tata Institute of Fundamental Research, Mumbai 400 005, India*
[g] *Oak Ridge National Laboratory, P.O. Box 2008, Oak Ridge, TN 37831, USA*

Received 29 November 2004; received in revised form 4 January 2005; accepted 13 January 2005

Abstract

The giant dipole resonance built on excited states was observed in very fissile nuclei in coincidence with evaporation residues. The reaction $^{48}Ca + ^{176}Yb$ populated evaporation residues of mass

* Corresponding author.
E-mail address: thoennessen@nscl.msu.edu (M. Thoennessen).
[1] Present address: Theragenics Corporation, 5203 Bristol Industrial Way, Buford, GA 30518, USA.
[2] Present address: Brookhaven National Laboratory, Upton, NY 11973-5000, USA.
[3] Present address: Department of Radiation Oncology, University of Michigan Hospitals and Health System, 1500 East Medical Center Drive, Box 0010, Ann Arbor, MI 48109, USA.
[4] Present address: JAERI Advanced Science Research Center, Japan.
[5] Permanent address: Kernfysisch Versneller Instituut, 9747 AA Groningen, The Netherlands.
✠ Deceased.

0375-9474/$ – see front matter
doi:10.1016/j.nuclphysa.2005.01.015

$A = 213$–220 with a cross section of ∼200 μb at 259 MeV. The extracted giant dipole resonance parameters are in agreement with theoretical predictions for this mass region.

PACS: 24.30.Cz; 25.60.Pj; 25.70.Jj; 27.90.+b

Keywords: NUCLEAR REACTIONS ^{176}Yb (^{48}Ca, X), $E = 206$, 219, 256, 259 MeV; measured E_γ, I_γ, (evaporation residue) γ-coin, γ-ray multiplicity and sum energy, fusion and evaporation residue σ. ^{224}Th deduced GDR parameters. Comparison with model predictions.

1. Introduction

The giant dipole resonance (GDR) built on highly excited states has been used extensively to study nuclear structure at finite temperatures and angular momenta [1]. In recent years it has also been useful for the investigation of reaction mechanisms in fusion-fission reactions [2]. The observation of excess high-energy γ-ray emission prior to fission [3,4] confirmed results from earlier pre-fission neutron measurements [5,6] that fission in hot systems is slower than expected from standard statistical model calculations.

The difficulty in these high-energy γ-ray experiments, in contrast to the neutron measurements, is the fact that it is not possible to distinguish experimentally the pre-fission γ-rays from γ-rays emitted from highly excited fission fragments. Measuring high-energy γ-rays in coincidence with evaporation residues eliminates this problem and would potentially give more detailed information about the dependence of the structure of these heavy nuclei as a function of temperature and angular momentum.

It also has been speculated that the spin distribution of the evaporation residues is an observable that can distinguish between the different possible causes of fission hindrance [7]. If the extra neutrons and high-energy γ-rays are emitted after the system has committed itself to fission, i.e., after the saddle point, the evaporation residue distribution will not be affected. However, if these particles are emitted earlier, the competition between particle emission and fission is altered and it could change the final spin distribution of the evaporation residues. A first measurement of the spin distribution following the decay of ^{194}Hg formed in the reaction $^{19}\mathrm{F} + {}^{175}\mathrm{Lu}$ showed no deviation from standard statistical model predictions, indicating that the fission hindrance does not occur in the presaddle region [8–10].

We chose the neutron deficient ^{224}Th for our studies because it is one of the most completely explored nuclei in terms of cross section and pre-fission γ-ray and light particle emission measurements. Fission [11–15] and evaporation residue cross section [14–17], as well as pre-fission neutron [18], charged particle [19] and γ-ray [3,20–23] measurements have been performed. Most of these studies utilized the reaction $^{16}\mathrm{O} + {}^{208}\mathrm{Pb}$ to populate the compound nucleus ^{224}Th. However, the detection efficiency of the evaporation residues with the light oxygen projectiles is rather small due to their small recoil energy. Thus we chose the reaction $^{48}\mathrm{Ca} + {}^{176}\mathrm{Yb}$ to form ^{224}Th.

2. Experimental setup and data analysis

The experiment was performed at Argonne National Laboratory (ANL) with the Argonne Tandem Linac Accelerator System (ATLAS). Beams of 206 MeV, 219 MeV, 256 MeV and 259 MeV ^{48}Ca bombarded an 810 μg/cm^2 thick ^{176}Yb target. The beam current was about 30 enA and the beam spot on the target was wobbled by an oscillating steering-magnet current in order to distribute the heating of the target [24].

The target was located in front of the fragment mass analyzer (FMA) [25] and was surrounded by the ANL-Notre Dame BGO array and the ORNL-MSU-TAMU BaF_2 array as shown in Fig. 1.

The target chamber was fabricated to allow the maximum closure of the BGO and BaF_2 packs. The beam-pipe was 1 inch in diameter up to the target and 2.5 inches between the target and FMA. The target chamber was wrapped in three foils to minimize low energy X-rays and reduce the overall count-rate in the BaF_2 detectors. The foils were 10 mil Ta, Cd, Cu. The chamber wall itself was 1/16 inch stainless steel.

Evaporation residues were detected with a position-sensitive parallel plate avalanche counter (PPAC) at the focal plane of the FMA, which disperses the residues according to their mass-to-charge ratio (M/Q). The acceptance opening angle of the FMA was 11° and the efficiency was ∼5%.

The γ-ray multiplicity and sum energy was recorded with the BGO array, consisting of 46 detectors which were mounted to closely surround the target as shown in Fig. 1.

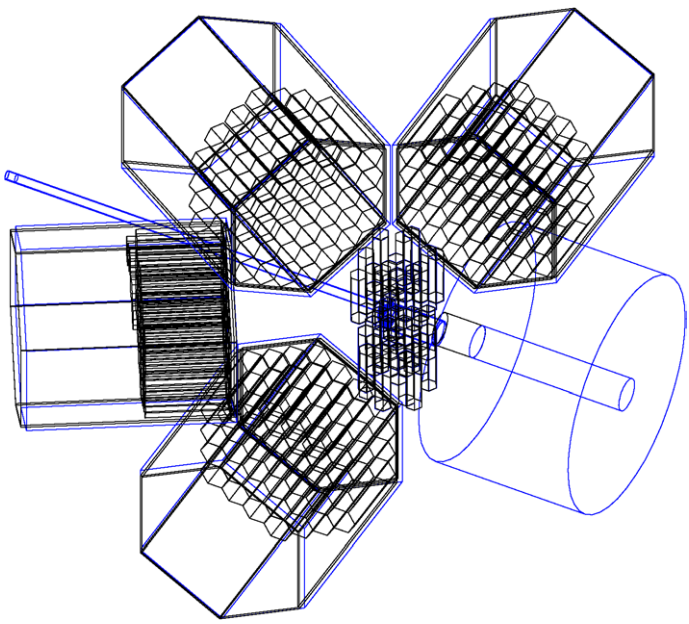

Fig. 1. Experimental setup of the BaF_2 array and the entrance quadrupole of the FMA with the multiplicity array closed around the target chamber.

High energy γ-rays from the reaction were measured with the BaF_2 array, consisting of 148 individual detectors. The BaF_2 crystals were set up in four packs of 37 crystals each. Each pack was hexagon shaped and closely-packed. The frame was an aluminum cage mounted horizontally with the center of the pack pointed toward the target as shown in Fig. 1. Two of the packs were located at 90°, and two at 121° located on either side of the beam. The front faces of the packs were 39 cm from the target. The upper and lower half of the BGO array were moved vertically for this measurement so that they would not block high-energy γ-rays in the BaF_2 array.

The BaF_2 detectors were calibrated with low energy γ-rays using a ^{88}Y (0.898 MeV and 1.836 MeV) and a ^{239}Pu^{13}C (6.13 MeV) source. Additional calibration points (4.44 MeV, 18.12 MeV and 22.56 MeV) were obtained from the ^{11}B(p,γ) reaction at $E_p = 7.2$ MeV. The energy resolution was ∼4% at 22.56 MeV. Neutron-γ-ray separation was achieved by time-of-flight and pulse shape discrimination was used to reject pile-up events. The response of the array was improved by a nearest neighbor sum of individual detectors. The complete response was simulated with GEANT [26].

3. Results

3.1. Evaporation residue cross section measurements

Evaporation residues were measured at beam energies of 206 MeV, 219 MeV and 259 MeV. The initial excitation energy (E^*) of the compound nucleus ^{224}Th calculated at the center of the target, the grazing angular momentum for fusion (l_g) and the fusion cross section ($\sigma_{\rm fus}$) calculating from the Bass model [27] for these three energies are listed in Table 1. The grazing angular momentum for fusion and the fusion cross section at the highest beam energy is limited by the vanishing fission barrier. Over 99% of the fusion cross section will lead to fission, with less than 1% leading to evaporation residues. Fig. 2 shows the measured total evaporation residue (solid bars) and 4n (open bars) cross sections for the reaction ^{48}Ca + ^{176}Yb. The largest uncertainty of the data is the overall efficiency of the FMA which was estimated to be 5%. The lengths of the (error)bars in Fig. 2 reflect this uncertainty. The overall cross section at 219 MeV is dominated by the 5n channel populating ^{219}Th, which has a lifetime of 1.05 μs [29]. This is comparable to the flight-time of the residues through the FMA (∼1.4 μs), resulting in a correction of a factor of 2 which has been included in Fig. 2. The 4n evaporation residue cross section agrees well with the measurement of reference [28] (open triangles). It should be noted that in reference [28]

Table 1
Beam energy ($E_{\rm lab}$), initial excitation energy (E^*) at the center of the target, grazing angular momentum for fusion (l_g) and fusion cross section ($\sigma_{\rm fus}$) for evaporation residue and γ-ray multiplicity measurements

$E_{\rm lab}$ (MeV)	E^* (MeV)	l_g ($\hbar$)	$\sigma_{\rm fus}$
206	41	36	150
219	52	63	415
259	83	74	1022

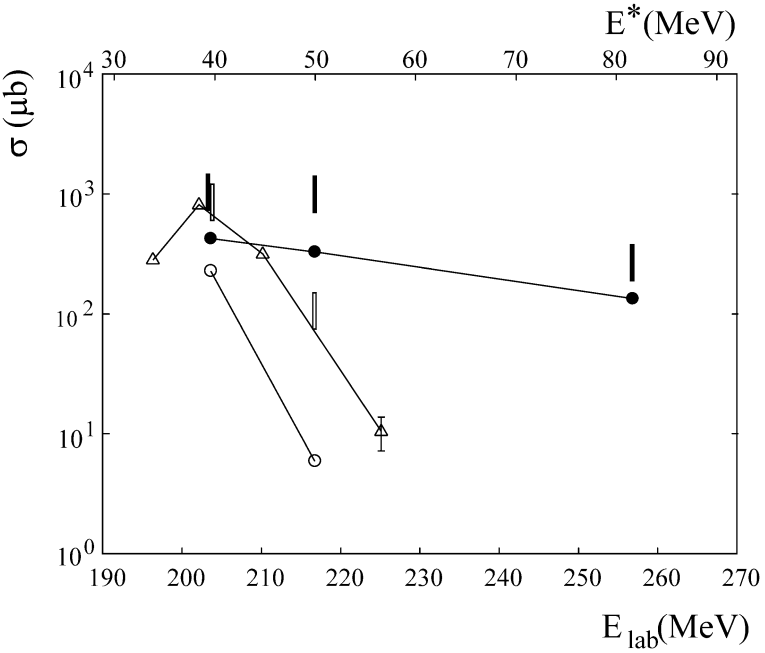

Fig. 2. Total (solid) and 4n (open) evaporation residue cross sections. The bars correspond to the present data, the triangles are data from Ref. [28] and the circles are from statistical model calculations.

there seems to be an inconsistency between the beam energies and derived excitation energies of ∼3 MeV. We chose the quoted beam energies in order to compare the two datasets based on a comparison of the other ^{48}Ca induced reactions measured in Ref. [28].

The measured evaporation residue cross sections are about a factor of ten smaller than the cross sections measured for the reaction $^{16}\mathrm{O} + {}^{208}\mathrm{Pb}$. The reduced fusion cross section for the ^{48}Ca induced reaction due to geometric effects can account for only a factor of two. The remaining difference could be due to an inhibition of fusion because of quasi-fission [30–32]. The initial mass asymmetry (defined as $\alpha = (M_T - M_P)/(M_T + M_P)$) of the $^{16}\mathrm{O} + {}^{208}\mathrm{Pb}$ reaction ($\alpha = 0.86$) is very close to the Businaro–Galone peak leading the projectile to be absorbed by the target. In contrast, in the more symmetric ($\alpha = 0.57$) $^{48}\mathrm{Ca} + {}^{176}\mathrm{Yb}$ reaction the projectile will gain mass inhibiting the fusion process [33,34].

Standard statistical model calculations using CASCADE [35,36] could not reproduce the measured large evaporation residue cross sections in the reaction $^{16}\mathrm{O} + {}^{208}\mathrm{Pb}$ [17]. The results of CASCADE calculations for the present reaction $^{48}\mathrm{Ca} + {}^{176}\mathrm{Yb}$ are also shown in Fig. 2. Standard input parameters were used: a diffuseness of the angular momentum distribution of $2\hbar$, a level density parameter of $a = 9$, and fission barriers from the Sierk [37] prescription. The ratio a_f/a_n was chosen to be unity. The solid and open circles represent the total and 4n evaporation residue cross sections, respectively. Both cross sections seem to be underpredicted. However, the accuracies of statistical model calculations are at best of the order of millibarns and certainly not microbarns. Rather small variations of the input parameters (fission barrier, level densities etc.) can result in large changes in the cross sec-

tion. Thus, without any additional experimental observables it is not possible to conclude that the evaporation residues measured for the $^{48}Ca + ^{176}Yb$ reaction are inconsistent with standard statistical model calculations. Because of the uncertainties of the statistical model calculations the present evaporation residue data do not allow us to conclude on the presence or absence of fission delay.

3.2. Multiplicity measurements

Another observable for potential deviations from standard statistical models are the spin distributions of the evaporation residues [7,8]. The BGO multiplicity filter was used to measure the entry distribution in excitation energy and angular momentum for the energies listed in Table 1. The dashed lines in Fig. 3 show the measured γ-ray multiplicities (left) and total γ-ray energy (right) for the three beam energies.

In order to compare the data to the results from statistical model calculation it is necessary to track in the calculation the specific decay paths leading to evaporation residues. The standard CASCADE code does not have this capability, instead, the Monte Carlo code

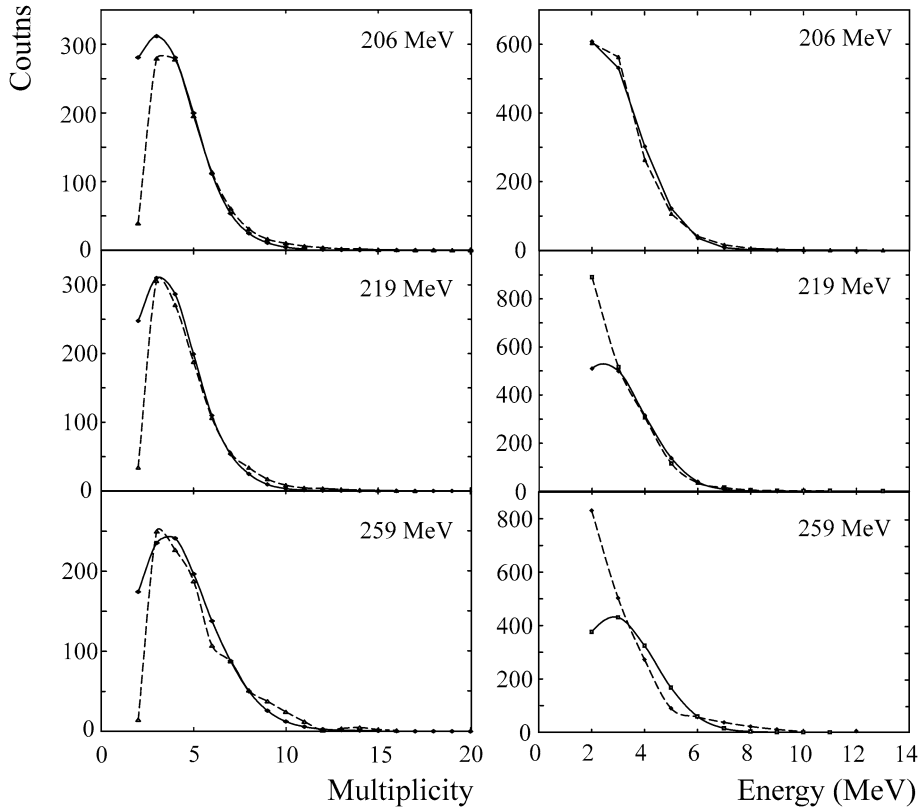

Fig. 3. Measured (dashed) and calculated (solid) γ-ray multiplicities (left) and total γ-ray energy (right) in coincidence with evaporation residues for beam energies of 206 MeV, 219 MeV and 259 MeV.

EvapOR [38] was used. EvapOR is an extension to the Hauser–Feshbach statistical-model code PACE2 [39]. Rather then unfolding the data, the calculations were folded with the energy and multiplicity response of the detector array, which was calculated using GEANT. The solid lines in Fig. 3 show the results of these calculations. The overall agreement of the multiplicity data is quite good, while there are deviations for the total energy spectra especially for the 259 MeV data.

The entry state distribution of the evaporation residues can then be extracted from EvapOR. Fig. 4 shows these calculated distributions for 206 MeV (dotted), 219 MeV (short-dashed) and 259 MeV (long-dashed). The contours correspond to the 50% level relative to the maximum of the distribution. The small fraction of the total fusion cross section leading to evaporation residues is limited to small angular momenta. All three distributions are rather similar with only a slight increase towards higher values for the higher beam energy. The calculated average angular momenta and sum energies are (12.9$\hbar$, 4.7 MeV), (13.5$\hbar$, 5.0 MeV), and (14.7$\hbar$, 6.4 MeV) for 206 MeV, 219 MeV and 259 MeV, respectively. The entry distributions for a single channel, ^{220}Th, have been measured [40] with the Gammasphere array at 206 and 219 MeV. They resemble, but are not in complete agreement with, the calculated results shown in Fig. 4, partly due to the fact that the calculations are for all evaporation residues.

The distributions are limited in energy by the fission barriers which are indicated for ^{220}Th (dotted) and ^{213}Ra (dashed) in Fig. 4. The Yrast line (solid line) was calculated from a fit to experimental data which has been measured up to 15$\hbar$ [41]. The lowest beam energy predominantly populates the 4n evaporation channel (^{220}Th) while the highest beam energy

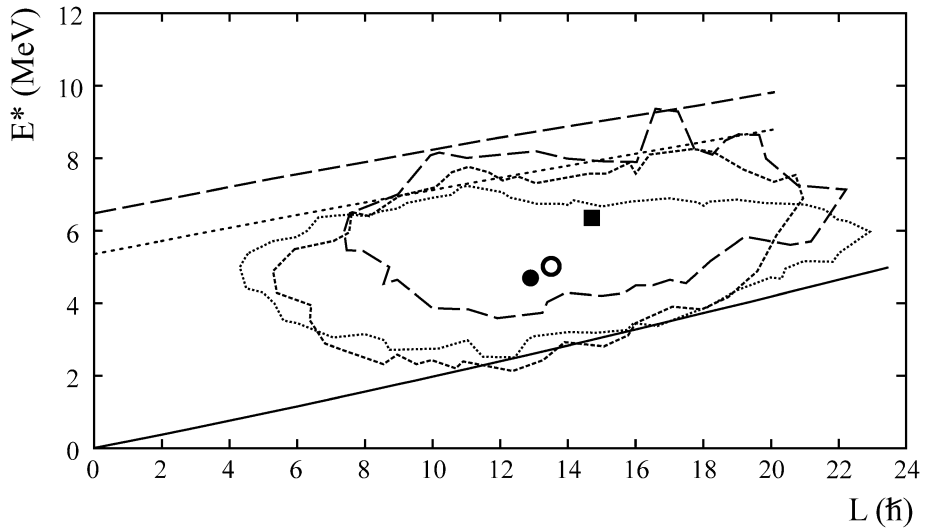

Fig. 4. Calculated entry state distributions for 206 MeV (dotted), 219 MeV (short-dashed) and 259 MeV (long-dashed). The contours correspond to the 50% level relative to the maximum of the distribution. The Yrast line (solid) and the fission barrier energies for ^{220}Th (dotted) and ^{213}Ra (long-dashed) are indicated. The location of the average entry in angular momentum and energy is shown by the solid circle (206 MeV), open circle (219 MeV), and solid square (259 MeV).

leads to the region of ^{213}Ra. The fact that the 259 MeV data populate evaporation residues at higher energies may be a result of α-particle emission leading to residues with a smaller charge and thus larger fission barriers. It should be mentioned that the fission barriers in this mass region are dominated by the liquid drop barriers and not by shell effects. In contrast, the fission barrier of ^{254}No, for which the entry distribution has been measured [24] is predominantly due to the shell-correction energy.

The overall good agreement of the multiplicity data at the three energies with standard statistical model calculations indicate that there is no need to introduce fission hindrance for these reactions at these energies. This then supports the recent observation that the observation of fission hindrance is due to effects beyond the saddle point [4,8].

3.3. Giant dipole resonance measurements

The measurement of the high-energy γ-rays was performed at a beam energy of 256 MeV. The multiplicity filter was retracted in order not to shield the BaF_2 detectors. Fig. 5 shows the γ-ray spectrum measured with the BaF_2 array in coincidence with evaporation residues in the FMA. An enhancement around 10 MeV where the GDR for nuclei in this heavy mass regions is expected is clearly visible. This corresponds to the observation of the GDR built on excited states in coincidence with evaporation residues in the heaviest system ever measured. The only other GDR γ-ray evaporation residue coincidence measurement in this mass region populated the hot compound nucleus ^{216}Rn [42].

In order to compare the spectrum with the results of theoretical predictions Monte Carlo calculations are necessary. Again the Monte Carlo code EvapOR was used to calculate and extract the high-energy γ-ray spectrum in coincidence with evaporation residues. The same standard statistical model parameters used for the calculations of the evaporation residues, γ-ray multiplicities and sum energies discussed in the previous sections were also used for the calculations of the high-energy spectra. Only a very small fraction of the total fusion cross section will result in evaporation residues ($< 0.1\%$) so it is fairly time consuming to generate a calculated γ-spectrum with reasonable statistics. In addition, the current data have also limited statistics so that it is not practical to try to fit the data by varying the GDR parameter.

Instead, calculations with previously used parameters were performed and compared to the data. Up to now the high energy γ-rays spectra from highly excited ^{224}Th were measured in coincidence with fission fragments. These spectra consisted of contributions from γ-rays emitted from the compound nuclear system prior to fission and γ-rays from the excited fission fragments [3]. More sophisticated analyses separated the pre-fission decay into contributions from the compound nucleus within the saddle point, emission from the saddle to scission point and decays from a mono-nucleus during the fast fission process [20–23].

Fig. 5 includes the results of three calculations. The calculations were normalized to the data over the whole energy range. The solid curve shows the spectrum with the parameters used in reference [23] of the GDR decay within the saddle point. A non-collective oblate shape ($\beta = -0.1$) for an excited liquid drop was assumed with $E_1 = 11.2$ MeV, $\Gamma_1 = 4.5$ MeV, $E_2 = 12.2$ MeV, $\Gamma_2 = 5.3$ MeV. The dashed line was calculated with the parameters of the saddle-to-scission decay $E_1 = 9.7$ MeV, $\Gamma_1 = 4.5$ MeV, $E_2 = 12.4$ MeV,

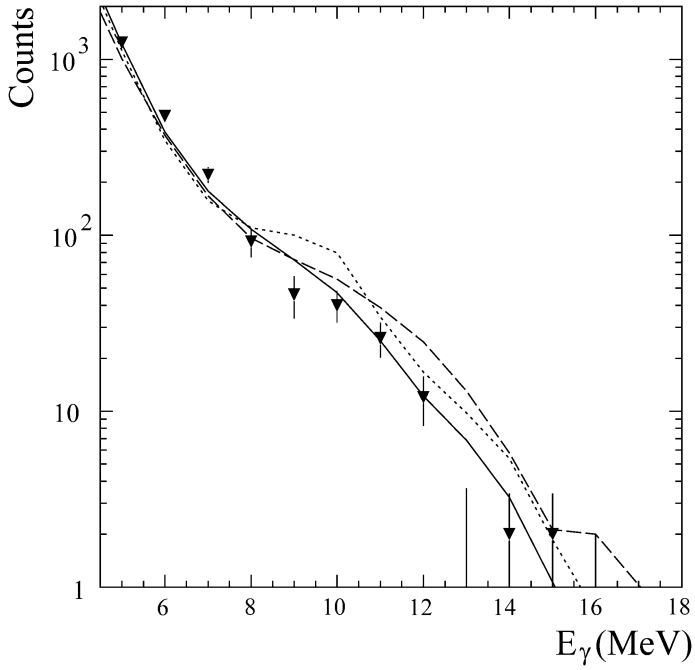

Fig. 5. High-energy γ-ray spectra in coincidence with evaporation residues compared to results from statistical model calculations assuming different deformations: $\beta = -0.1$ (solid), $\beta = 0.3$ (dashed) and $\beta = 0.56$ (dotted).

$\Gamma_2 = 7.3$ MeV corresponding to prolate deformed nucleus ($\beta = 0.3$). The dot-dashed curve represents parameters of an even larger prolate deformation ($\beta = 0.56$) for the decay of the mono nucleus: $E_1 = 9.8$ MeV, $\Gamma_1 = 2.5$ MeV, $E_2 = 15.5$ MeV, $\Gamma_2 = 5.0$ MeV [20].

All calculations were folded with the detector response which was simulated by GEANT [26] and included the full geometry of the experimental setup and the nearest neighbor sum which was used for the data. The latter two calculations clearly do not agree with the measurements especially in the region of the compound nucleus GDR. This is not surprising because the data in coincidence with evaporation residues should not contain contributions from the fission path. The first calculation describes the data fairly well justifying the choice of parameters for the compound nucleus pre-fission contribution of reference [23]. The fact that the data can be explained solely with γ-ray emission from non-collective oblate shapes, indicates that it is not influenced by the fission competition. This is again consistent with the interpretation that the fission hindrance originates predominantly from the path between the saddle and the scission point [4].

4. Conclusion

The fusion evaporation reaction ^{48}Ca on ^{176}Yb was used to study highly excited compound nuclei of ^{224}Th. The evaporation residue cross section measurement did not exhibit any large excess relative to standard statistical model calculations. The measured multi-

plicities and the total energies are also consistent with the statistical model. The GDR built on highly excited states was observed for the first time in such a heavy nucleus in coincidence with evaporation residues. The shape of the highly excited fused system is consistent with a non-collective oblate shape. The present results are consistent with the interpretation that the previously observed fission delay occurs predominantly between the saddle and scission point and not inside the saddle point.

Acknowledgements

This work has been supported by the National Science Foundation grant number PHY01-10253 and by the US Department of Energy under number W-31-109-ENG-3. K.E. acknowledges the support of the Research Experience for Undergraduates (REU) program by the National Science Foundation and Student Research Participation Program at Argonne National Laboratory.

References

[1] P.F. Bortignon, A. Bracco, R.A. Broglia, Nuclear Structure at Finite Temperature, Harwood Academic, Amsterdam, 1998.
[2] P. Paul, M. Thoennessen, Annu. Rev. Nucl. Part. Sci. 44 (1994) 65.
[3] M. Thoennessen, D.R. Chakrabarty, M.G. Herman, R. Butsch, P. Paul, Phys. Rev. Lett. 59 (1987) 2860.
[4] N.P. Shaw, I. Diószegi, I. Mazumdar, A. Buda, C.R. Morton, J. Velkovska, J.R. Beene, D.W. Stracener, R.L. Varner, M. Thoennessen, P. Paul, Phys. Rev. C 61 (2000) 044612.
[5] A. Gavron, A. Gayer, J. Boissevain, H.C. Britt, T.C. Awes, J.R. Beene, B. Cheynis, D. Drain, R.L. Ferguson, F.E. Obenshain, F. Plasil, G.R. Young, G.A. Petitt, C. Butler, Phys. Rev. C 35 (1987) 579.
[6] D. Hilscher, H. Rossner, Ann. Phys. (Paris) 17 (1992) 471.
[7] M. Thoennessen, J.R. Beene, Phys. Rev. C 45 (1992) 873.
[8] S.K. Hui, et al., Phys. Rev. C 62 (2000) 054604.
[9] I. Diószegi, Phys. Rev. C 64 (2001) 019801.
[10] S.K. Hui, et al., Phys. Rev. C 64 (2001) 019802.
[11] F. Videbaek, R.B. Goldstein, L. Grodzins, S.G. Steadman, T.A. Belote, J.D. Garrett, Phys. Rev. C 15 (1977) 954.
[12] P. Sperr, H. Essel, J.J. Koerner, K.E. Rehm, Z. Phys. A 291 (1979) 179.
[13] B.B. Back, R.R. Betts, K. Cassidy, B.G. Glagola, J.E. Gindler, L.E. Glendenin, B.D. Wilkins, Phys. Rev. Lett. 52 (1984) 397.
[14] C.R. Morton, D.J. Hinde, J.R. Leigh, J.P. Lestone, M. Dasgupta, J.C. Mein, J.O. Newton, H. Timmers, Phys. Rev. C 52 (1995) 243.
[15] C.R. Morton, A.C. Berriman, M. Dasgupta, D.J. Hinde, J.O. Newton, K. Hagino, I.J. Thompson, Phys. Rev. C 60 (1999) 044608.
[16] E. Vulgaris, L. Grodzins, S.G. Steadman, R. Ledoux, Phys. Rev. C 33 (1986) 2017.
[17] K.-T. Brinkmann, A.L. Caraley, B.J. Fineman, N. Gan, J. Velkovska, R.L. McGrath, Phys. Rev. C 50 (1994) 309.
[18] H. Rossner, D.J. Hinde, J.R. Leigh, J.P. Lestone, J.O. Newton, J.X. Wei, S. Elfstrom, Phys. Rev. C 45 (1992) 719.
[19] B.J. Fineman, K.-T. Brinkmann, A.L. Caraley, N. Gan, R.L. McGrath, J. Velkovska, Phys. Rev. C 50 (1994) 1991.
[20] R. Butsch, D.J. Hofman, C.P. Montoya, P. Paul, M. Thoennessen, Phys. Rev. C 44 (1991) 1515.
[21] I. Diószegi, D.J. Hofman, C.P. Montoya, S. Schadmand, P. Paul, Phys. Rev. C 46 (1992) 627.

[22] D.J. Hofman, B.B. Back, P. Paul, Phys. Rev. C 51 (1995) 2597.
[23] I. Diószegi, N.P. Shaw, I. Mazumdar, A. Hatzikoutelis, P. Paul, Phys. Rev. C 61 (2000) 024613.
[24] P. Reiter, et al., Phys. Rev. Lett. 84 (2000) 3542.
[25] C.N. Davids, B.B. Back, K. Bindra, D.J. Henderson, W. Kutschera, T. Lauritsen, Y. Nagame, P. Sugathan, A.V. Ramayya, W.B. Walters, Nucl. Instrum. Methods B 70 (1992) 358.
[26] Detector description and simulation tool GEANT, version 3.21, CERN Program Library, Geneva.
[27] R. Bass, Phys. Rev. Lett. 39 (1977) 265.
[28] C.-C. Sahm, H.-G. Clerc, K.-H. Schmidt, W. Reisdorf, P. Armbruster, F.P. Hessberger, D. Vermeulen, Nucl. Phys. A 441 (1985) 316.
[29] O. Häusser, W. Witthuhn, T.K. Alexander, A.B. McDonald, J.C.D. Milton, A. Olin, Phys. Rev. Lett. 31 (1973) 323.
[30] B.B. Back, Phys. Rev. C 31 (1985) 2104.
[31] J. Toke, R. Bock, G.X. Dai, A. Gobbi, S. Gralla, K.D. Hildenbrand, J. Kuzminski, W.F.J. Müller, A. Olmi, H. Stelzer, B.B. Back, S. Bjornholm, Nucl. Phys. A 440 (1985) 327.
[32] J.P. Blocki, H. Feldmeier, W.J. Swiatecki, Nucl. Phys. A 459 (1986) 145.
[33] K.T.R. Davies, A.J. Sierk, Phys. Rev. C 31 (1985) 915.
[34] A.C. Berriman, D.J. Hinde, M. Dasgupta, C.R. Morton, R.D. Butt, J.O. Newton, Nature 413 (2001) 144.
[35] F. Pühlhofer, Nucl. Phys. A 280 (1977) 267.
[36] R. Butsch, M. Thoennessen, D.R. Chakrabarty, M.G. Herman, P. Paul, Phys. Rev. C 41 (1990) 1530.
[37] A.J. Sierk, Phys. Rev. C 33 (1986) 2039.
[38] N.G. Nicolis, J.R. Beene, EvapOR, a multi-particle Monte Carlo evaporation code, 1993, unpublished.
[39] A. Gavron, Phys. Rev. C 21 (1980) 230.
[40] A. Heinz, et al., Nucl. Phys. A 682 (2001) 458c.
[41] W. Bonin, H. Backe, M. Dahlinger, S. Glienke, D. Habs, E. Hanelt, E. Kankeleit, B. Schwartz, Z. Phys. A 322 (1985) 59.
[42] M. Kmiecik, et al., Phys. Rev. C 70 (2004) 064317.